Direct~~In-situ~~ observation for RH−dependent mixing states of submicron particles containing organic surfactants and inorganic salts

Chun Xiong[1#], Binyu Kuang[1#], Fei Zhang[1], Xiangyu Pei[1], Zhengning Xu[1], Zhibin Wang[1,2,3*]

[1]College of Environmental and Resource Sciences, Zhejiang University, Zhejiang Provincial Key Laboratory of Organic Pollution Process and Control, Hangzhou, 310058, China

[2]ZJU-Hangzhou Global Scientific and Technological Innovation Center, Zhejiang University, Hangzhou 311215, China

[3]Key Laboratory of Environment Remediation and Ecological Health, Ministry of Education, Zhejiang University, Hangzhou, 310058, China

Correspondence to Zhibin Wang (wangzhibin@zju.edu.cn)

[#] Chun Xiong and Binyu Kuang contribute equally to this work.

Abstract: Aerosol mixing state plays an important role in heterogeneous reactions and CCN activity. Organic surfactants could affect aerosol mixing state through bulk−surface partitioning. However, the mixing state of surfactant containing particles remains unclear due to the lack of direct measurements. Here, direct ~~in-situ~~ characterizations of mixing state for 20 kinds of submicron particles containing inorganic salts (NaCl and $(NH_4)_2SO_4$) and atmospheric organic surfactants (organosulfates, organosulfonates, and dicarboxylic acids) were conducted upon relative humidity (RH) cycling by Environmental Scanning Electron Microscopy (ESEM). As RH increased, surfactant shells inhibited water diffusion exposing to inorganic core, leading to notably increased inorganic deliquescence RH (88.3−99.5%) compared with pure inorganic aerosol. Meanwhile, we directly observed obvious Ostwald ripening process, that is, the growth of larger crystals at the expense of smaller ones, in 6 among 10 NaCl−organic surfactants systems. As a result of water inhibition by organic surfactant shell, Ostwald ripening in all systems occurred at RH above 90%, which were higher than reported RH range for pure NaCl measured at 27℃ (75−77%). As RH decreased, 8 systems underwent liquid−liquid phase separation (LLPS) before efflorescence, showing a strong dependence on organic molecular oxygen−to−carbon ratio (O:C). Quantitatively, LLPS was always observed when O:C ≤ 0.43 and was never observed when O:C > ~0.57. Separation RH (SRH) of inorganic salt−organic surfactant mixtures generally followed the trend of $(NH_4)_2SO_4$ < NaCl, which is consistent with their salting out efficiencies reported in previous studies. Solid phase separations were observed after efflorescence for systems without LLPS. Our results provide a unique insight into the consecutive mixing processes of the inorganic salt−organic surfactant particles, which would help improve our fundamental knowledge of model development on radiative effect.

1 Introduction

Atmospheric particles are complex mixtures of multiple inorganic and organic matters (Pöschl, 2005). When relative humidity (RH) varies, particles can undergo phase transitions such as deliquescence (Peng et al., 2001), efflorescence (Takahama et al., 2007), and liquid−liquid phase separation (LLPS) (Martin, 2000), hence altering mixing state. The transition of aerosol mixing state can influence gas uptake, hygroscopicity, cloud condensation nuclei (CCN) activity, and radiative absorption (Riemer et al., 2019).

Upon hydration, previous studies suggested that different mixing state between inorganic and organic matters influence aerosol hygroscopic behaviours (e.g., deliquescence) and solar radiation (Peng et al., 2016; Li et al., 2021). For instance, Peng et al. (2016) observed internal mixed NaCl−oxalic acid deliquesced at 73% RH, being slightly lower than that of pure NaCl (75%) because of the interactions between inorganic and organic matters. However, Li et al. (2021) found a different deliquescence process if ammonium sulfate (AS) was coated by secondary organic aerosol, the organic shell firstly dissolved at ~50% RH but water uptake of the AS core was inhibited, leading to a higher deliquescence RH of AS (~83−90%). By cryogenic transmission electron microscopy (cryo−TEM), Zhang et al. (2022) directly observed collected particles from a rural site remained LLPS (inner inorganic p 0has e and outer organic phase) between organic matter and inorganic salts when RH raised to 75 ± 2% and 86 ± 2%, but LLPS disappeared when RH increased to 95 ± 2%. They later suggested that LLPS with higher ratio of organic coating thickness to black carbon size can drive black carbon from inorganic core to organic particle coatings, which could result in 18% radiative absorption overestimation of black carbon aerosols in climate models by assuming a core-shell particle structure.

Upon dehydration, phase separation has been frequently observed in ambient particles (You et al., 2012; Ting et al., 2018; Zhang et al., 2020; Zhang et al., 2022). For example, LLPS occurred at > 90% RH for particles containing water extraction of collected atmospheric particles in Atlanta and simulations indicated that LLPS can decrease particle uptake of N_2O_5 thus increase concentrations of gas−phase NO_3 and N_2O_5 (You et al., 2012). Factors contributing to LLPS, e.g. oxidation levels (Bertram et al., 2011; Song et al., 2017; Song et al., 2019), organic fraction (Ciobanu et al., 2009; Song et al., 2012a), inorganic species (You et al., 2013), and temperature (You and Bertram, 2015; Roy et al., 2020) have been discussed for some specific inorganic−organic or organic−organic systems in literature. Song et al. (2012b) and You et al. (2013) found LLPS always occurred for O:C < ~0.5, never occurred for O:C > 0.8, and when O:C was between 0.5 and 0.8, LLPS was depended on inorganic species. Organic fraction showed controversial effects on LLPS (Bertram et al., 2011; Song et al., 2012a) since Bertram et al. (2011) found a weak effect of organic fraction on LLPS for 8 out of 11 AS−organic systems but the rest systems exhibited a quantifiable dependence of separation RH (SRH) on organic fraction. You et al. (2013) reported SRH among out of 20 organics generally followed the trend of $(NH_4)_2SO_4 \geqslant NH_4HSO_4 \geqslant NaCl \geqslant NH_4NO_3$, which is consistent with

inorganic salting out efficiencies. Temperature did not strongly affect SRH between 253−290 K for AS−organics (O'brien et al., 2015; You and Bertram, 2015) and NaCl−organics systems (Roy et al., 2020). Recently, dry rate (Altaf and Freedman, 2017; Altaf et al., 2018) and size effect (Freedman, 2020; Ott and Freedman, 2021; Ohno et al., 2023) on LLPS were found for submicron particles. Undergoing drying by fast rate (~ 27% per minute), phase separation of AS-pimelic acid system occurred in larger particles (75 ~ 322 nm diameter), but smaller particles (below 25~135 nm diameter) were homogeneous. In slow drying rates (0.04 to 0.08% RH per second), particles with diameter below 43 nm were homogeneous but larger particles (28 ~ 629 nm) were mainly phase-separated (Altaf and Freedman, 2017). Freedman (2020) further explained that LLPS is scarcely occurred in smaller particles as smaller particles cannot overcome the energy barrier needed to form a new phase.

Dicarboxylic acids (Ruehl and Wilson, 2014), organosulfates (Bruggemann et al., 2020; Reed et al., 2022), and organosulfonates (Bruggemann et al., 2020; Guo et al., 2020) are important organic constituents in secondary organic aerosol. Primary emission and secondary transition were major sources of dicarboxylic acids and their mass contribution of dicarboxylic acids to total particulate carbon exceeds 10% (Römpp et al., 2006; Ho et al., 2010; Hyder et al., 2012). Organosulfates and organosulfonates, as significant reservoirs of sulfur, comprise an estimated 5%–30% of the total organic aerosol mass (Tolocka and Turpin, 2012; Reed et al., 2022). Above mentioned organics contain both hydrophilic (e.g., sulpho group) and hydrophobic groups (e.g., alkyl group), showing surface activity and causing bulk−surface partitioning (Noziere, 2016; Ruehl et al., 2016), hence affecting individual aerosol morphology (Kwamena et al., 2010). However, mixing state of submicron inorganic salt−organic surfactant particles remain unclear due to the lack of direct measurements. Here, we directly observed mixing states of submicron particles containing inorganic salt and organic surfactant with varying organic volume fraction (OVF) upon humidity cycling by Environmental Scanning Electron Microscopy (ESEM). Our results could provide unique insights into the dynamic evolution of inorganic salt−organic surfactant particles under fluctuating atmospheric conditions.

2 Materials and Methods

2.1 Chemicals

NaCl and AS were purchased from Sinopharm chemical reagent (purity ≥ 99.8%) and Sigma Aldrich (purity ≥ 99 %), respectively. The studied organic substances include 10 surface active organics (five organosulfonates, three organiosulfates and two dicarboxylic acids). The five organic sulfonates were sodium propane sulfonate ($C_3H_7SO_3Na$), sodium butane sulfonate ($C_4H_9SO_3Na$), sodium pentane sulfonate ($C_5H_{11}SO_3Na$), sodium heptane sulfonate ($C_7H_{15}SO_3Na$), sodium octane sulfonate ($C_8H_{17}SO_3Na$). The three organic sulfates were sodium methyl sulfate (CH_3SO_4Na), sodium ethyl sulfate ($C_2H_5SO_4Na$) and sodium octyl sulfate ($C_8H_{17}SO_4Na$). Two dicarboxylic acids were pimelic acid (PA) and phenylmalonic acid (PhMA). Relevant properties of used chemicals were summarized in **Table 1.** These organic surfactants were of various solubilities, from sparingly soluble (e.g., 0.07 mol L^{-1} for $C_8H_{17}SO_4Na$) to highly soluble (e.g., 2.6 mol L^{-1} for CH_3SO_4Na).

O:C ratios were from 0.38 to 4, covering most of the molar ratios in the atmosphere (0.1−1.0) (You et al., 2013). The studied organic substances contain functional groups such as sulfonates, sulfates, carboxylic acids and aromatics, which were universally detected in atmospheric aerosol samples (Takahama et al., 2007).

Table 1 Organic surfactants and their relevant properties investigated in this study.

Species	Compounds	Formula	*Solubility (mol L^{-1})	O:C	Purity	Supplier
Organic sulfonate	Sodium propane sulfonate	$C_3H_7SO_3Na$	2.5	1.00	>98%	Aladdin
	Sodium butane sulfonate	$C_4H_9SO_3Na$	2.4	0.75	≥99%	Aladdin
	Sodium pentane sulfonate	$C_5H_{11}SO_3Na$	0.8	0.60	98%	Aladdin
	Sodium heptane sulfonate	$C_7H_{15}SO_3Na$	0.6	0.43	98%	Macklin
	Sodium octane sulfonate	$C_8H_{17}SO_3Na$	0.07	0.38	≥99%	Macklin
Organic sulfate	Sodium methyl sulfate	CH_3SO_4Na	2.6	4.00	98%	Energy Chemical
	Sodium ethyl sulfate	$C_2H_5SO_4Na$	1.5	2.00	98%	Meryer
	Sodium octyl sulfate	$C_8H_{17}SO_4Na$	0.2	0.50	99%	Rhawn
Dicarboxylic acid	Pimelic acid (PA)	$C_7H_{12}O_4$	0.3	0.57	99%	Macklin
	Phenylmalonic acid (PhMA)	$C_9H_8O_4$	0.2	0.44	98%	Aladdin

* https://comptox.epa.gov/ (last access: 19 Jun, 2023)

2.2 Aerosol generation and collection

The process of aerosol generation and collection was detailly described by Xiong et al. (2022). In brief, particles were nebulized from solutions of organic and inorganic matters (~5 g L^{-1}) mixed with deionized water (Millipore, resistivity = 18.2 MΩ). After drying (RH < 15%) by a silica-gel diffusion dryer, particles were deposited with an eight stage non−viable particle sizing sampler (Models BGI20800 Series, BGI Incorporation) onto 400 mesh copper grids coated with carbon films (Zhongjingkeyi Films Technology Co. Ltd.). Copper grids were mounted on the 7^{th} stage, selecting particles with aerodynamic

size of 0.7−1 μm. Collected samples were stored under dry condition (RH < 10%) and were immediately characterized within 24 hours to avoid possible sample aging.

2.3 Mixing state observation

Optical microscopy (Ciobanu et al., 2009; Bertram et al., 2011; Song et al., 2012a, b; You et al., 2013), microfluidic device (Roy et al., 2020), Cryo-TEM (Veghte et al., 2014; Freedman, 2020; Ott and Freedman, 2021; Ott et al., 2021; Zhang et al., 2022), ESEM (O'brien et al., 2015), optical tweezer (Stewart et al., 2015; Tong et al., 2022)and F-AFT (Fluorescence aerosol flow tube) (Ohno et al., 2021; Ohno et al., 2023) were reported methods for detecting aerosol mixing state in the literature. Optical microscopy and microfluidic device were commonly used direct method for substrate-supported droplets but was limited by size range (at least dozens of micrometers). Optical tweezer and F-AFT could investigated LLPS in a levitated micrometer and sub-micrometer droplet, respectively, but are indirect ways, although no distinct differences when comparing to substrate-supported droplets (Ohno et al., 2023). Cryo-TEM and ESEM could detect mixing state in sub-micrometer scale but damage caused by electron beam may exist (depend on chemistry and beam parameters settings). Ott et al. (2021) give some useful suggestions in minimize the damage, e.g., decreasing exposure dose and time to particles.

Mixing state was observed by Environmental Scanning Electron Microscopy (ESEM, Thermo Quattro S) with a temperature−controlled stage. The RH in chamber was varied between 0.1 to ~ 25 ℃, and controlled by adjusting the temperature (± 0.1 ℃) at a predefined pressure (610 Pa). In each experiment, particles with lateral dimensions of ~ 1 μm were selected first (based on the deposition, volume-equivalent size was smaller than 1 μm). Then the RH raised from low (~ 30%) to high condition (~100%) at the change rate of 2−3% RH min^{-1}. High RH lasted for at least 5 minutes for equilibrium, promising complete dissolution (O'brien et al., 2015). With increased RH, most selected particles grew larger to several micrometers before subsequent LLPS experiment. Then, RH decreased to dry condition at similar change rate. Negligible influence on the LLPS of AS−organic (O'brien et al., 2015; You and Bertram, 2015) and NaCl−organic systems (Roy et al., 2020) in micrometre scale (from several micrometers to dozens of micrometers). Cloud parcel modelling suggests that atmospheric RH fluctuations typically occur from 0 to 3.6% min^{-1} (Pöhlker et al., 2014). Therefore, we assume that the water uptake in our experiments approximates atmospheric conditions (Shiraiwa et al., 2013). Images of mixing states during the whole RH period were acquired at an electron acceleration voltage of 30 kV. The detector used for the ESEM imaging was a scanning transmission electron detector. The images were recorded with line scanning rates of 3−5 μs to minimize the possible beam damage (Supporting information, O'brien et al., 2015). The varying range of RH value between two consecutive pictures were mostly 0.2−0.4% RH (very narrow), in order to capture the possible quick transitions of mixing states. Each image in our study contained at least 5 particles (or droplets) to ensure the ESEM reproducibility and decrease the uncertainty. In addition, we have repeated some of the experiment (e.g., in the RH decreasing period) for reproducibility validation, and the results showed good consistence (**Fig. S1**).

3 Results and Discussion

3.1 Mixing states upon hydration

Deliquescence RH (DRH) and Efflorescence RH (ERH) of pure NaCl (**Fig. 1a−d** and **Fig. S2a−b**) and AS particles (**Fig. 2a−d** and **Fig. S2c−d)** were firstly tested via the experimental setup. DRH of NaCl and AS were observed at 80.9 ± 0.1% (literature: 77 ± 1% (Pöhlker et al., 2014)) and 82.1± 0.6% (literature: 82.0% (Onasch et al., 1999)). ERH of NaCl and AS were 48.3 ± 0.4% (literature: 48 ± 2% (Zeng et al., 2014)) and 30.7 ± 0.9% (literature: 31 ± 1% (Cheng and Kuwata, 2023)). Generally, the experimental DRH and ERH values correspond well with those in literature, confirming the reliability of the experimental setup. DRH of NaCl showed slight deviation by about nearly 4%, which could be explained by kinetic effects when the system had not reached full equilibrium (Pöhlker et al., 2014). Before deliquescence, the substrate-supported NaCl and AS particles both showed substantial water uptake, forming an aqueous halo around a solid core. Similar observational results of NaCl and AS have been reported, and could be explained by interactions at the sample/substrate interface, which plays an important role in such gradual phase transition as additional energy term (Wise et al., 2008; Pöhlker et al., 2014).

Figure 1e and Fig. 2e illustrate the two separated phases with dark core (blue arrow) and bright shell (green arrow) of dry deposited NaCl−$C_2H_5SO_4Na$ and AS−$C_2H_5SO_4Na$ particles. The dark cores are indicated to be inorganics, because darker regions are characteristic of areas with higher atomic number elements (e.g., Cl) and/or a thicker sample region (Laskin et al., 2006; O'brien et al., 2015). Phase separations with core−shell structure were observed for all studied inorganic salt−organic surfactant systems. This may be attributed to the size range of particles we investigated (~ 1 μm with dry lateral dimension), since inorganic salt−organic surfactant particles with such size range might overcome the energy barrier needed to form a new phase (Altaf and Freedman, 2017; Altaf et al., 2018; Freedman, 2020; Ott and Freedman, 2021). According to results in Freedman (2020), morphology of most systems were found size-dependent, where large particles were phase-separated and small particles were homogeneous. Furthermore, all systems (e.g, AS–PA and AS–succinic acid systems) with dry diameters larger than 0.7 μm were observed phase-separated no matter the occurrence of size dependence (Altaf and Freedman, 2017). Freedman (2020) expected that phase-separation could be attributed by nucleation and growth, therefore larger particles tended to be phase-separated morphology. In another study, Ohno et al. (2021) also found that LLPS occurred at lower RH in smaller droplet (70 – 190 nm) than in larger droplet (260 – 370 nm).

When RH increased from dry, as organic phase slowly absorbed water, NaCl and AS cores were not fully dissolved at RH of 90.1% and 91.7% (**Fig. 1g and Fig. 2g**), respectively, being notably higher than their DRH. The phenomenon was found for all NaCl−organic surfactant and AS−organic surfactant systems and the DRH of the inorganic salts were ranged in 88.3−99.5% (**Fig. 1i and Fig. 2i**). Laskina et al. (2015) measured the DRH of pure AS and NaCl at submicrometer (100 nm) and supermicrometer (3−10 μm) size ranges by hygroscopic tandem differential mobility analyzers (HTDMA) and MicroRaman Spectroscopy, respectively, and the deviations between them were both within 3%, indicating that DRH of pure AS and NaCl showed weak size dependence (> 100 nm). In addition, Cheng and Kuwata (2023) used low-temperature

hygroscopicity tandem differential mobility analyzer (Low−T HTDMA) and observed consistent DRH of NaCl and AS within experimental error under temperature ranged in −10 ℃ to 22.5 ℃, suggesting that the DRH of NaCl and AS experience a neglect temperature dependence. According to the above-mentioned studies, DRH of pure AS and NaCl displayed weak dependence on size (> 100 nm) and temperature, and we therefore concluded that surfactant shell inhibits water diffusion exposing to inorganic cores, resulting in delays of deliquescence of inorganic cores.The inhibition of surfactant shell could be triggered by increased viscosity with raised RH, since reported studies have reported that organic shells can transform form solid to semisolid with high viscosity at wet condition (Zhang et al., 2018). In a RH-constrained lab study at constant room temperature, Li et al. (2021) also observed organic coating of secondary organic aerosol (oxidizing α-pinene) started to deliquesce first, but the phase changes of AS cores from solid to liquid took place at 83−90% RH, lower than those in the current study. This was possibly caused by the water diffusion coefficient through organic phase, which could be affected by organic species and environment parameters such as temperature. Given by Nguyen et al. (2017), the diffusion coefficient of a water molecule through an organic shell could be decreased by lower temperature. In the current study, higher RH in the ESEM chamber was achieved by decreasing temperature, thus might decrease diffusion coefficient of water in organic surfactant and lead to higher DRH than those in Li et al. (2021). Previous study and the current work indicated the phenomenon (water inhabitation by organic coating) to be a common and important procedure in affecting ambient aerosol hygroscopicity, because inorganic−organic core−shell structures were ubiquitous observed in field (Li et al., 2016; Unga et al., 2018; Xu et al., 2020; Li et al., 2021; Wang et al., 2021; Zhang et al., 2022). Though the water inhabitation of organic shell in the current study was observed at temperature much lower than room temperature, it is meaningful and may affect aerosol properties in some special area such as polar regions (Lambert et al., 2013; Kirpes et al., 2022; Zavacka et al., 2022) or winter time period (Xu et al., 2021; Zhang et al., 2021) where are characteristic with low-temperature environment.

As previous study believed that deliquescence on hydration for inorganics independent of circumstances, **Fig. 3** illustrates an unexpected phase transition of NaCl cores coated with $C_2H_5SO_4Na$. As shown in **Fig. 3a**, a droplet with several NaCl cores was observed at 97.0% RH since discussed above that organic shell inhibits water diffusion. NaCl cores in droplet were a bigger one (marked by white square) and the rest were smaller. When RH gradually raised (**Fig. 3b**−**c**), as smaller NaCl cores serially deliquesced and dissolved, the size of the bigger NaCl core surprisingly increased, indicating a simultaneous NaCl recrystallization at the expense of smaller ones (i.e., Ostwald ripening) (Boistelle and Astier, 1988). After other small particles totally dissolve, the bigger NaCl core deliquesced and fully dissolved at 99.5% RH (**Fig. 3d**). A previous study reported "efflorescence upon hydration" for 1:1 mixed NaCl-gluconic acid and AS-gluconic acid by optical tweezer (Zhu et al., 2022). Based on IR spectrum, they found the coexistence of partial efflorescence mixed state, ultraviscous state and liquid state during "efflorescence upon hydration" period, indicating an unstable crystal and concentrated liquid state of NaCl. In this circumstance, Ostwald ripening can take place. Ostwald ripening was triggered by the decrease of total system free energy, since dissolved small and effloresced big crystals reduce the total system free energy (Voorhees, 1985). We directly and observed obvious Ostwald ripening processes in 6 among 10 NaCl−organic surfactants systems. As a results of water inhibition

by surfactant shell discussed above, Ostwald ripening here all occurred at RH above 90%, which were notably higher than reported 75%−77% for pure NaCl measured by X-ray microspectroscopy at 27℃ (Pöhlker et al., 2014).

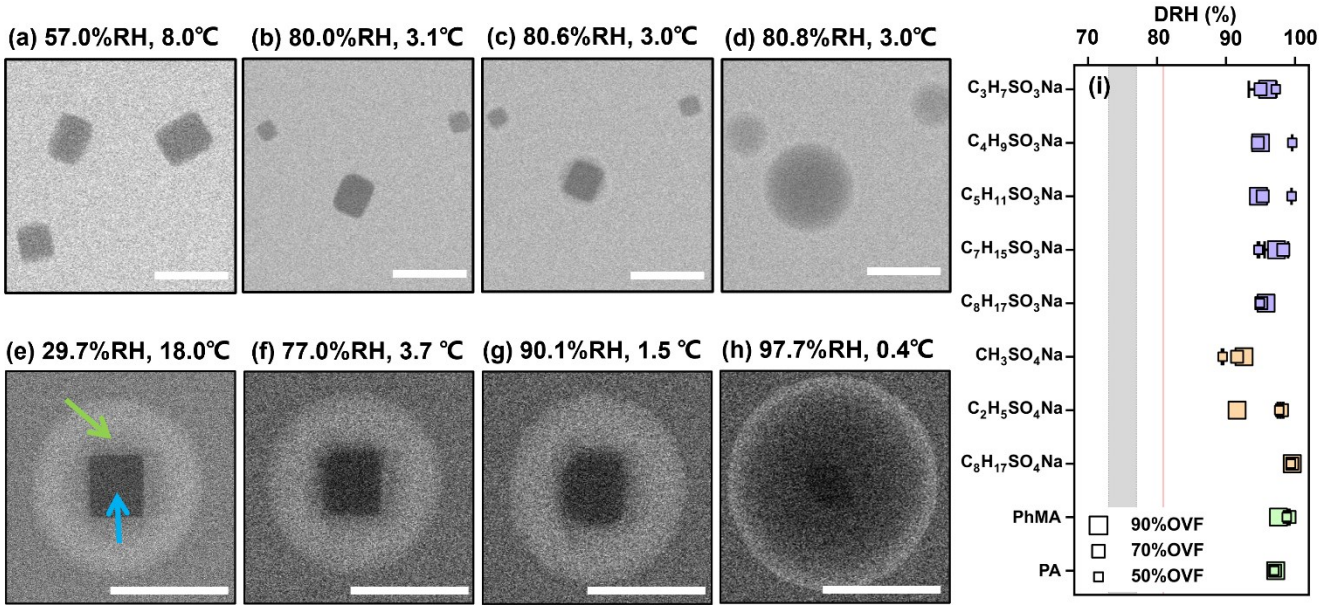

Figure 1. ESEM images of (a−d) pure NaCl and (e−h) NaCl−$C_2H_5SO_4Na$ (70% OVF) with different RH. Blue and green arrows indicate the inorganic phase and organic phase, respectively. The RH value that NaCl core fully dissolved (DRH) for NaCl−organic surfactant systems with different OVF (i). Grey area in (i) covers DRH range of NaCl in the literature obtained from Peng et al. (2022). Red line indicates the measured average DRH of pure NaCl (80.9 ± 0.1%). Scale bars in (a-h) were 1 μm.

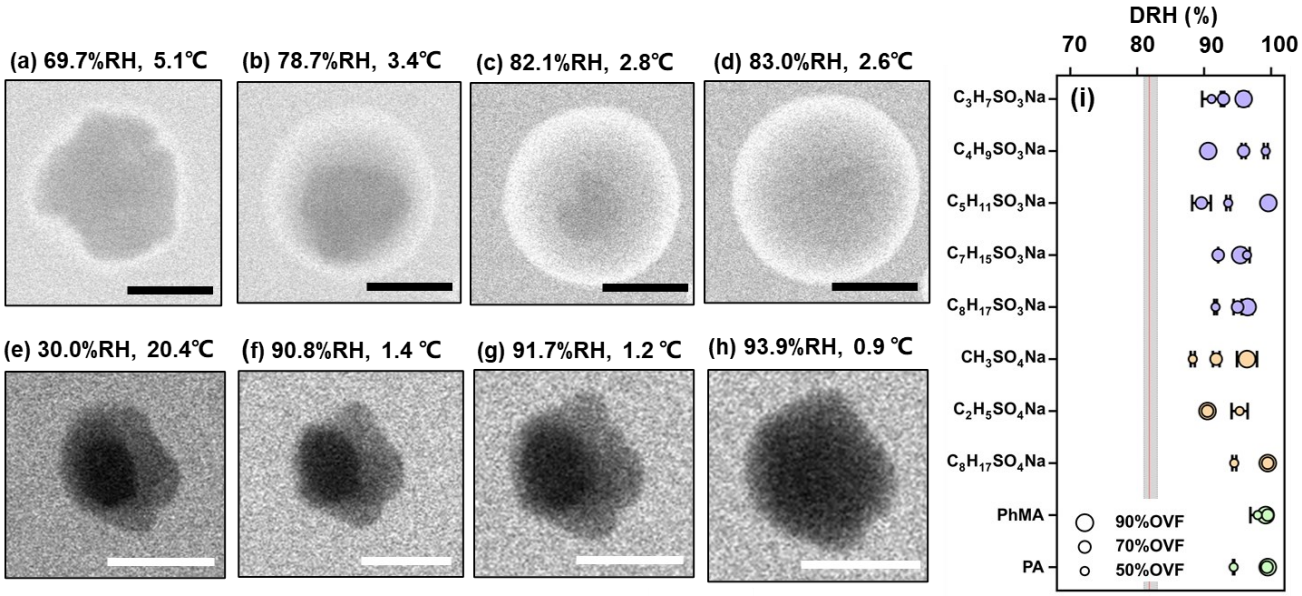

Figure 2. ESEM images of (a−d) pure AS and (e−h) AS−$C_2H_5SO_4Na$ (50% OVF) with different RH. Blue and green arrows indicate the inorganic phase and organic phase, respectively. The RH value that AS core fully dissolved (DRH) for AS−organic surfactant systems with different OVF (i). Grey area in (i) covers DRH range of AS in the literature obtained from Peng et al. (2022). Red line indicates the measured average DRH of pure AS (82.1 ± 0.6%). Scale bars in (a-h) were 1 μm.

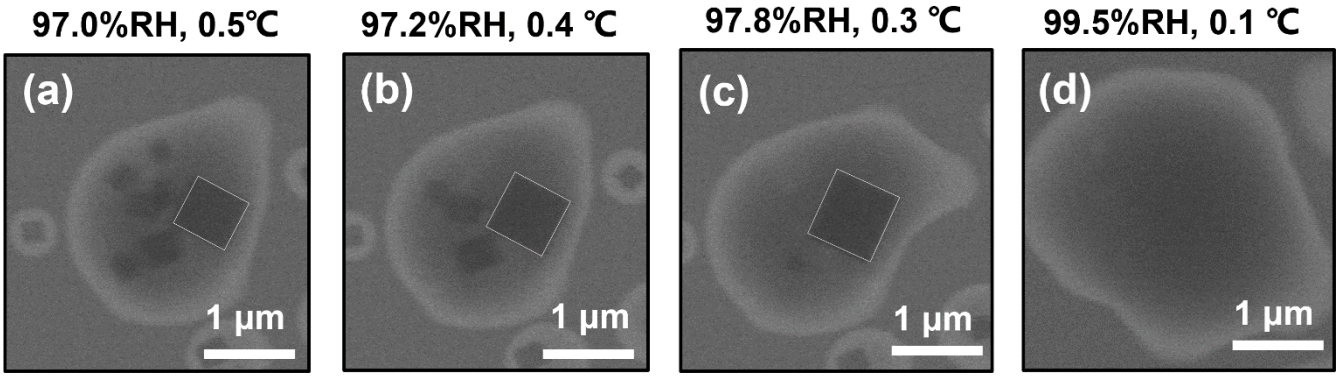

Figure 3. ESEM images of Ostwald ripening for NaCl−$C_8H_{17}SO_4Na$ (50% OVF) particle. White square indicates the biggest NaCl core (assumed square) in droplet. The biggest NaCl grew larger (recrystallization) while the small NaCl cores dissolved.

3.2 Mixing states upon dehydration

LLPS

In **Fig. 4a**, AS−$C_8H_{17}SO_4Na$ was homogeneous under RH of 99.5%. When RH decreased to 98.2%, the particles showed two separated liquid phases (i.e., LLPS) with a dark inner phase and a light outer phase (**Fig. 4b**), which were highlighted by the blue and green arrows. In addition, the AS−$C_8H_{17}SO_4Na$ remained LLPS when RH continue to decline until efflorescence of inner inorganic phase occurred (**Fig. 4c**). In our study, 8 among 20 chemical systems underwent LLPS, including 4 AS−organic surfactant systems and 4 NaCl−organic surfactant systems. **Fig. 5** illustrates the relationship between LLPS occurrence and molar ratios (O:C and H:C) of the surface−active organics, as well as reported results of other binary inorganic salt−organic systems in literature (Bertram et al., 2011; You et al., 2013; You and Bertram, 2015). In our study, LLPS always occurs when the O:C ratio is below 0.43 (yellow dashed line in **Fig. 5**) for NaCl–organic surfactant and AS–organic surfactant droplets. This value was close to the reported values in You et al. (2013) (~ 0.5). However, in their results, LLPS was never observed when O:C was above ~ 0.8 (grey dashed line in **Fig. 5**) (Bertram et al., 2011; Song et al., 2012b; You et al., 2013),which was higher than that in our experiment (0.57). We ascribe this to the insufficient chemical systems in our experiment (10 systems), which was notably smaller than in previous studies (over 30). As a result, the bounds of O:C determining LLPS were not changed if our results were added in previous studies such as You et al. (2013) and Song et al. (2012b).

In order to analyze the effect of inorganic salts in LLPS, we compared SRH of systems which contained same organic matters but different inorganic salts. Results showed that SRH of AS−$C_8H_{17}SO_4Na$ (70% OVF), AS−$C_8H_{17}SO_3Na$ (90% OVF), AS−PhMA (90% OVF) and AS−PA (90% OVF) were 98.7 ± 0.5%, 81.3 ± 1.2%, 97.9 ± 1.0% and 98.5 ± 0.8%, and were all notably higher than SRH of corresponding NaCl−containing systems (92.5 ± 3.9%, 56.4 ± 1.2%, 85.6 ± 3.6% and 66.7 ± 0.8%), respectively. This was attributed to different salting out efficiency of inorganic salts, since You et al. (2013) found the SRH of inorganic−organic mixtures followed the trend of $(NH_4)_2SO_4 \geq NH_4HSO_4 \geq NaCl \geq NH_4NO_3$, which were generally consistent with their salting out efficiency.

The measured SRH values as a function of OVF are plotted in **Fig. 6**. AS−$C_8H_{17}SO_4Na$ showed SRH of 98.7 ± 0.5% when OVF was 70%, higher than those of 50% OVF (82.1 ± 1.6%) and 90% OVF (80.0 ± 0.9%). However, the phenomenon was totally different from that of AS−$C_8H_{17}SO_3Na$, which showed lower SRH with 70% OVF (62.2 ± 2.6%) than those of 50% OVF (69.6 ± 1.0%) and 90% OVF (81.3 ± 1.2%). Therefore, the above results indicated controversial effect of OVF on SRH (Bertram et al., 2011; Song et al., 2012a).

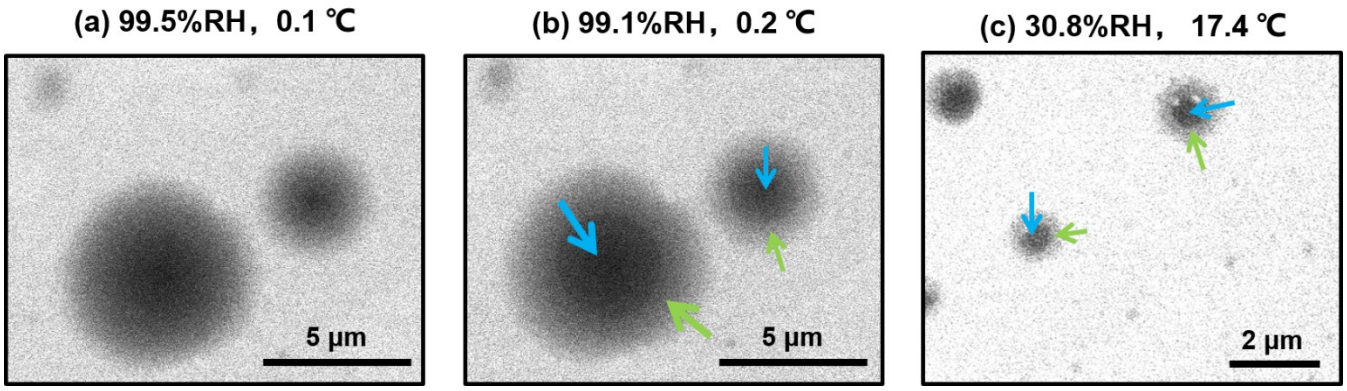

252

253

254 **Figure 4.** ESEM images of (a) homogeneous AS−$C_8H_{17}SO_4Na$ particles (70% OVF) underwent (b) LLPS and (c) efflorescence.

255

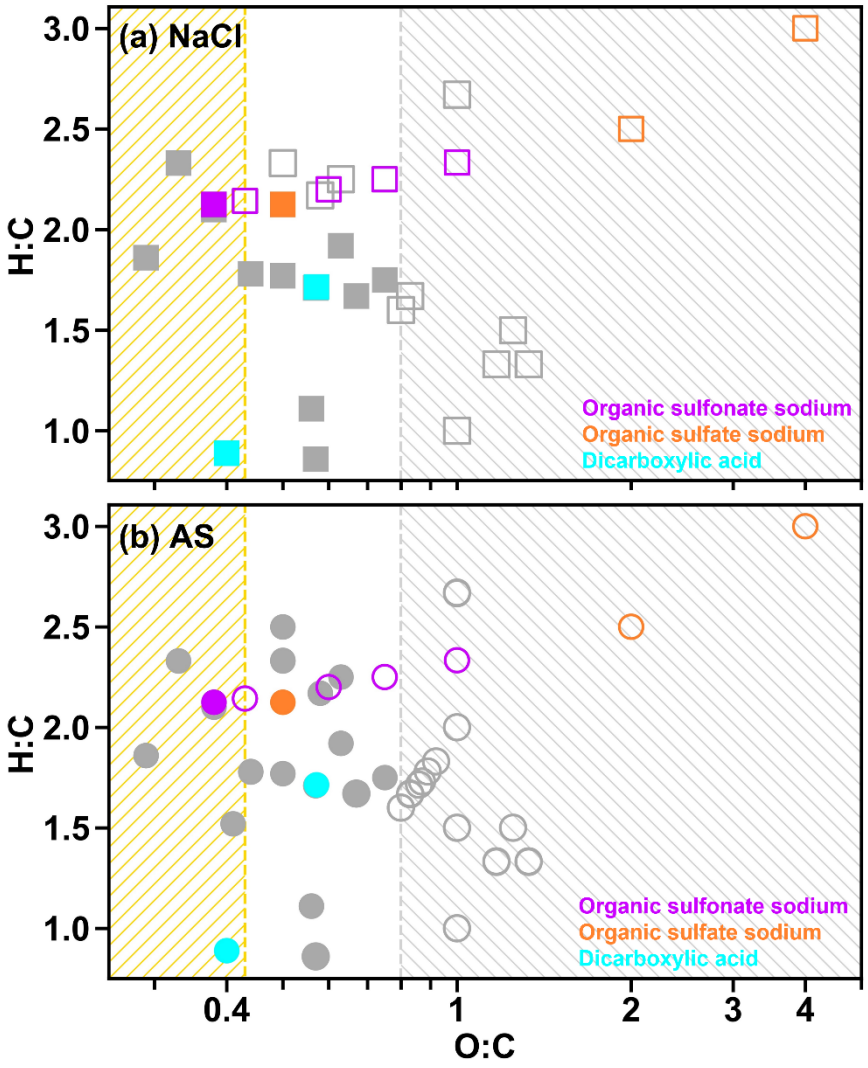

Figure 5. Van Krevelen Diagram for the mixed inorganic−surfactants particles in the current study (symbols in red, orange and cyan): (a) NaCl−organic surfactant and (b) AS−organic surfactant systems. Solid symbols indicate that LLPS was observed for particles with at least one OVF, while hollow symbols indicate that LLPS was not observed for particles with all OVFs. Symbols in grey in (a) and (b) were results obtained from Bertram et al. (2011), You et al. (2013) and You and Bertram (2015). Yellow-hatched region (O:C < 0.43) means that LLPS observed in all investigated systems, while grey-hatched region (O:C > 0.8) means no LLPS detected in any of the investigated systems.

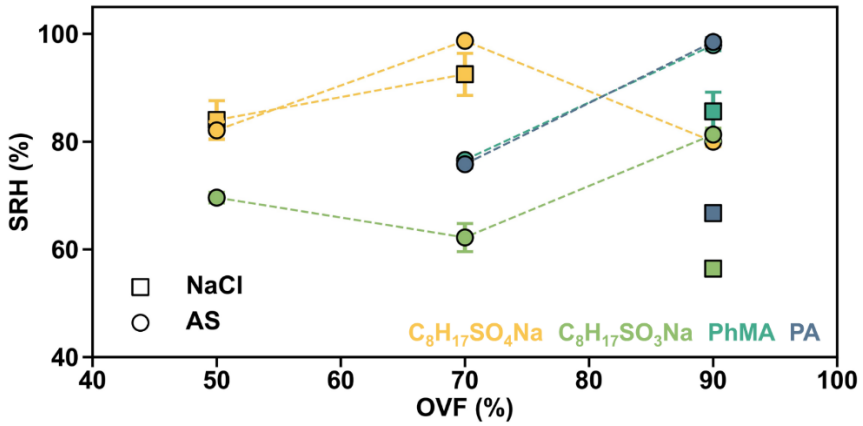

Figure 6. Summary of SRH results as a function of OVF for inorganic-surfactant particles.

Solid phase separation

For mixed systems without undergoing LLPS, we found they were separated with distinct core−shell phases from homogeneous morphology at low RH. However, this phase transition was different from LLPS, since the inner phase was with irregular shape (LLPS occurred with rounded inner liquid phase), which was attributed to the efflorescence progress of inorganic salt (**Fig. 7**). Therefore, we termed it solid phase separation. The efflorescence RH (ERH) of inner inorganic salt, therefore, was the solid phase separation RH.

In **Fig. 8a**, ERH of NaCl−organic surfactant particles with 50%, 70% and 90% OVF were ranged in 47.0−61.8%, which was higher than the measured ERH (48.3 ± 0.4%) and reported ERH range of pure NaCl (41−51%) (Peng et al., 2022). This could be explained by the interaction between organic and inorganic matters. For example, Ghorai et al. (2014) found an acid displacement reaction in NaCl−glutaric acid systems, which was driven by gaseous HCl liberation and causing chloride depletion. Such interactions of chloride depletion may facilitate efflorescence transitions, resulting in efflorescence at ~ 68% RH and ~ 60% RH, respectively, for internally mixed NaCl−glutaric acid particles with molar ratios of 1:3 and 1:1. Higher ERH could also be attributed to heterogeneous nucleation initiated by chemical purities (Choi and Chan, 2002). Choi and Chan (2002) observed 54.4% ERH for a 1:1mixed NaCl−glutaric acid, and they explained that insoluble additives crystallized and formed nuclei for the heterogeneous efflorescence of inorganic salts, leading to their higher ERH values.

As for AS−organic surfactant systems (**Fig. 8b**), efflorescence was observed for 27 among 30 aerosol samples. We did not observe distinct occurrence of efflorescence for the rest 3 samples, and 2 samples among 3 were with 90% OVF, which could be explained by the possible loss of AS when it was persistently exposed to electronic beam (Posfai et al., 2013; O'brien et al., 2015), especially for particles in which inorganic fractions were small (i.e., high OVF). ERH values of AS−organic surfactant particles with 50%, 70%, and 90% OVF ranged in 31.2−46.6%, showing a close result to the reported ERH of pure AS (30−48%) (Peng et al., 2022), but higher than the measured ERH (30.7 ± 0.9%). The potential cause may be the heterogeneous crystallization of AS on organic salts (Wang et al., 2019; Yang et al., 2019; Ma et al., 2021). For example, Wang et al. (2019) investigated the efflorescence of AS in AS−sodium oxalate and found SRH values were 48.9% and 55.3% with organic-inorganic mole ratios of 1:1 and 3:1, respectively, which were higher than that of pure AS (47.5%). Likely, Yang et al. (2019) also observed that the initial ERH of AS rose to 47.7% and 62% for inorganic mole ratios 1:3 and 1:1 AS−sodium pyruvate mixtures, respectively.

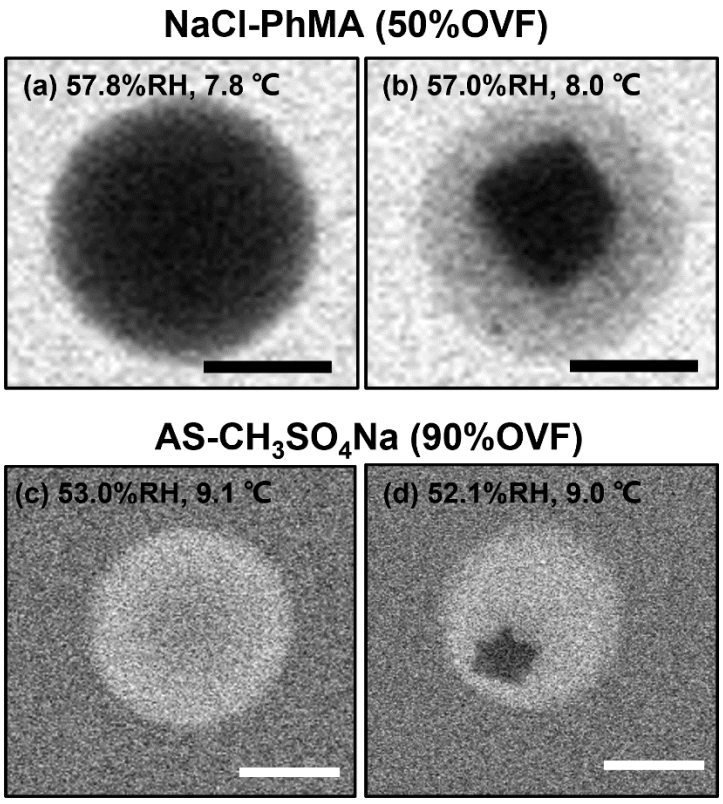

Figure 7. ESEM images of solid phase separation for (a−b) NaCl−PhMA and (c−d) AS−CH_3SO_4Na systems. The scale bars in (a-d) were 500 nm.

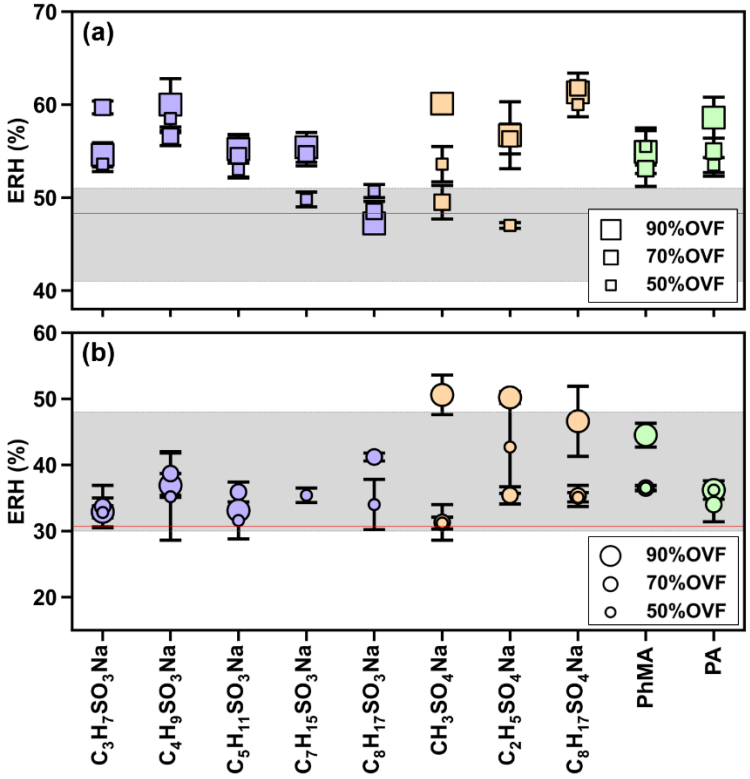

Figure 8. Measurements of efflorescence relative humidity (ERH) of (a) NaCl−organic surfactant and (b) AS−organic surfactant particles. The grey areas in (a) and (b) indicate the efflorescence RH range of NaCl (41−51%) and AS (30−48%) obtained from Peng et al. (2022). Red lines in (a) and (b) represent the measured average ERH of pure NaCl (48.3 ± 0.4%) and AS (30.7 ± 0.9%).

3.3 Atmospheric implication

Dicarboxylic acids, organosulfates, and organosulfonates are important surface−active organic constituents in secondary organic aerosol. Few studies comprehensively studied their mixing state upon fluctuating RH cycling, which is a simulate of real atmospheric condition. In this work, we concluded that mixing state affected interactions of inorganic salt with water. Since common assumptions in chemical transport models (including ISORROPIA-II (Fountoukis and Nenes, 2007), EQSAM (Metzger et al., 2002a; Metzger et al., 2002b), and MOSAIC (Zaveri et al., 2008)) are that water uptake is determined separately by the inorganic compounds and organics (i.e., the effect of mixing state was ignored) (Myhre et al., 2007; Nandy et al., 2021), thereby our results implied further effect of mixing states on estimations of aerosol hygroscopicity (e.g., growth factor), optical properties, and radiative forcing.

During dehydration, we investigated phase−separated before and after efflorescence for inorganic salts−organic surfactant

particles. Compared with homogeneous particles, phase−separated particles could decrease trace gas uptake (You et al., 2012), resulting in reduction of the formation of secondary organic aerosols (SOAs) (Zhang et al., 2018). In addition, organic phase was enriched in "outer shell", which can potentially alter aerosol water activity and lower aerosol surface tension, hence affecting aerosol−cloud interactions because water uptake of organic matter in current models (e.g. MPMPO (Griffin et al., 2003) and SOA treat-ment in CMAQ v5.2 (Pye et al., 2017)) is estimated by highly parameterized relationships assuming ideal solutions, e.g., using the kappa hygroscopicity parameter with water surface tension (Petters and Kreidenweis, 2007; Nandy et al., 2021).

Our results provide comprehensive information of mixing states between inorganic salts and organic surfactant in nanoscale perspective, which could help the establish of incorporation atmospheric modeling, to improve predictions on indirect effects of aerosol−climate interactions. We should note that in the atmosphere most particles are smaller (e.g., 0.1 to 0.3 μm) than sample particles and the chemical characteristics of ambient aerosol are not as simple as binary chemical systems in the current study. Therefore. the water kinetic inhibition should be further investigated for smaller particles containing more complex systems in the future.

4 Conclusions

Atmospheric surfactants have potential to distribute to surface, altering mixing state hence influencing aerosol hygroscopicity and CCN activity. But currently direct observation of RH−depended mixing state of aerosol containing atmospheric surfactants is scarce. In this study, dynamic mixing state and phase transitions of 20 types of submicron particles containing inorganic and surface−active organic constituents were directly investigated upon relative humidity (RH) cycling by Environmental Scanning Electron Microscopy (ESEM).

Inorganic-organic core-shell morphology was found for dry deposited mixed inorganic salt-organic surfactant particles. During hydration, organic shell inhibited water diffusion exposing to inorganic cores, resulting in higher deliquescence RH (88.3−99.5%) of inner inorganic phase compared with pure inorganic aerosol. This was because higher RH may facilitate phase transition of organic shell from solid to semisolid, raising organic viscosity thus decreasing water diffusion exposing to inorganic core. Meanwhile, we directly observed obvious Ostwald ripening of NaCl, that is, the growth of larger NaCl crystal at the expense of smaller ones, in 6 among 10 NaCl−organic surfactant systems. As a result of water inhibition by surfactant shell, Ostwald ripening in all systems occurred at RH above 90%, which were higher than reported RH range of pure NaCl measured at 27℃ (75−77%).

During dehydration, 8 among 20 chemical systems underwent LLPS, including 4 AS−organic surfactant systems and 4 NaCl−organic surfactant systems. LLPS was always observed when O:C ≤ 0.4 and never been observed when O:C > ~0.57. SRH values of AS−organic surfactant particles were generally higher than SRH of corresponding NaCl−organic surfactant systems, which was consistent with reported salting out efficiency of inorganic salts. OVF showed a controversial effect on SRH of inorganic salt−organic surfactant systems. Additionally, inorganic salt−organic surfactant systems without LLPS

underwent solid phase separation after efflorescence and also showed distinct separated phases. Our results provide a comprehensive and unique insights into the dynamic evolution of inorganic salt−organic surfactant particles under fluctuating atmospheric conditions, which could help improve our fundamental knowledge and decrease uncertainty of model estimation on global radiative effect.

***Data availability*.** The experiment data are available at ZENODO (https://doi.org/10.5281/zenodo.8079001)

Author contributions. CX and BK did the experiments, analyzed data. CX plotted the figures and wrote the original draft. FZ and XP contributed to discussion and reviewed the manuscript. BK and ZX reviewed the manuscript and contributed to the fund acquisition. ZW administrated the project, conceptualized the study, reviewed the manuscript and contributed to fund acquisition.

Financial support. The research was supported by National Natural Science Foundation of China (91844301, 41805100, 42005087, and 42005086) and the Key Research and Development Program of Zhejiang Province (2021C03165 and 2022C03084).

Acknowledgment. We thank Yuzhong Zhang from School of Engineering, Lin Liu and Wenjing Cao from Instrumentation and Service Center for Physical Sciences at Westlake University for the supporting in ESEM experiments.

***Competing interests*.** The authors declare no competing financial interest.

Reference

Altaf, M. B. and Freedman, M. A.: Effect of Drying Rate on Aerosol Particle Morphology, J. Phys. Chem. Lett., 8, 3613-3618, https://doi.org/10.1021/acs.jpclett.7b01327, 2017.

Altaf, M. B., Dutcher, D. D., Raymond, T. M., and Freedman, M. A.: Effect of Particle Morphology on Cloud Condensation Nuclei Activity, ACS Earth Space Chem., 2, 634-639, https://doi.org/10.1021/acsearthspacechem.7b00146, 2018.

Bertram, A. K., Martin, S. T., Hanna, S. J., Smith, M. L., Bodsworth, A., Chen, Q., Kuwata, M., Liu, A., You, Y., and Zorn, S. R.: Predicting the Relative Humidities of Liquid-Liquid Phase Separation, Efflorescence, and Deliquescence of Mixed Particles of Ammonium Sulfate, Organic Material, and Water Using the Organic-to-Sulfate Mass Ratio of the Particle and the Oxygen-to-Carbon Elemental Ratio of the Organic Component, Atmos. Chem. Phys., 11, 10995-11006, https://doi.org/10.5194/acp-11-10995-2011, 2011.

Boistelle, R. and Astier, J. P.: Crystallization Mechanisms in Solution, J. Cryst. Growth, 90, 14-30, https://doi.org/10.1016/0022-0248(88)90294-1, 1988.

Bruggemann, M., Xu, R. S., Tilgner, A., Kwong, K. C., Mutzel, A., Poon, H. Y., Otto, T., Schaefer, T., Poulain, L., Chan, M. N., and Herrmann, H.: Organosulfates in Ambient Aerosol: State of Knowledge and Future Research Directions on Formation, Abundance, Fate, and Importance, Environ. Sci. Technol., 54, 3767-3782, https://doi.org/10.1021/acs.est.9b06751, 2020.

Cheng, M. Q. and Kuwata, M.: Development of the Low-Temperature Hygroscopicity Tandem Differential Mobility Analyzer (Low-T HTDMA) and its Application to $(NH_4)_2SO_4$ and NaCl Particles, J. Aerosol Sci., 168, 106111, https://doi.org/10.1016/j.jaerosci.2022.106111, 2023.

Choi, M. Y. and Chan, C. K.: The Effects of Organic Species on the Hygroscopic Behaviors of Inorganic Aerosols, Environ. Sci. Technol., 36, 2422-2428, https://doi.org/10.1021/es0113293, 2002.

Ciobanu, V. G., Marcolli, C., Krieger, U. K., Weers, U., and Peter, T.: Liquid-Liquid Phase Separation in Mixed Organic/Inorganic Aerosol Particles, J. Phys. Chem. A, 113, 10966-10978, https://doi.org/10.1021/jp905054d, 2009.

Fountoukis, C. and Nenes, A.: ISORROPIA II: a computationally efficient thermodynamic equilibrium model for K^+-Ca^{2+}-Mg^{2+}-NH_4^+-Na^+-SO_4^{2-}-NO_3^--Cl^--H_2O aerosols, Atmos. Chem. Phys., 7, 4639-4659, https://doi.org/10.5194/acp-7-4639-2007, 2007.

Freedman, M. A.: Liquid-Liquid Phase Separation in Supermicrometer and Submicrometer Aerosol Particles, Acc. Chem. Res., 53, 1102-1110, https://doi.org/10.1021/acs.accounts.0c00093, 2020.

Ghorai, S., Wang, B. B., Tivanski, A., and Laskin, A.: Hygroscopic Properties of Internally Mixed Particles Composed of NaCl and Water-Soluble Organic Acids, Environ. Sci. Technol., 48, 2234-2241, https://doi.org/10.1021/es404727u, 2014.

Griffin, R. J., Nguyen, K., Dabdub, D., and Seinfeld, J. H.: A coupled hydrophobic-hydrophilic model for predicting secondary organic aerosol formation, J. Atmos. Chem., 44, 171-190, https://doi.org/10.1023/A:1022436813699, 2003.

Guo, L. Y., Peng, C., Zong, T. M., Gu, W. J., Ma, Q. X., Wu, Z. J., Wang, Z., Ding, X., Hu, M., Wang, X. M., and Tang, M. J.: Comprehensive Characterization of Hygroscopic Properties of Methanesulfonates, Atmos. Environ., 224, 117349, https://doi.org/10.1016/j.atmosenv.2020.117349, 2020.

Ho, K. F., Lee, S. C., Ho, S. S. H., Kawamura, K., Tachibana, E., Cheng, Y., and Zhu, T.: Dicarboxylic acids, ketocarboxylic acids, α-dicarbonyls, fatty acids, and benzoic acid in urban aerosols collected during the 2006

406 Campaign of Air Quality Research in Beijing (CAREBeijing-2006), J. Geophys. Res.: Atmos., 115, D19312,
407 https://doi.org/10.1029/2009jd013304, 2010.
408 Hyder, M., Genberg, J., Sandahl, M., Swietlicki, E., and Jönsson, J. Å.: Yearly trend of dicarboxylic acids in organic
409 aerosols from south of Sweden and source attribution, Atmos. Environ., 57, 197-204,
410 https://doi.org/10.1016/j.atmosenv.2012.04.027, 2012.
411 Kirpes, R. M., Lei, Z. Y., Fraund, M., Gunsch, M. J., May, N. W., Barrett, T. E., Moffett, C. E., Schauer, A. J.,
412 Alexander, B., Upchurch, L. M., China, S., Quinn, P. K., Moffet, R. C., Laskin, A., Sheesley, R. J., Pratt, K.
413 A., and Ault, A. P.: Solid organic-coated ammonium sulfate particles at high relative humidity in the
414 summertime Arctic atmosphere, Proc. Natl. Acad. Sci. U.S.A., 119, https://doi.org/10.1073/pnas.2104496119,
415 2022.
416 Kwamena, N. O. A., Buajarern, J., and Reid, J. P.: Equilibrium Morphology of Mixed Organic/Inorganic/Aqueous
417 Aerosol Droplets: Investigating the Effect of Relative Humidity and Surfactants, J. Phys. Chem. A, 114, 5787-
418 5795, https://doi.org/10.1021/jp1003648, 2010.
419 Lambert, F., Kug, J. S., Park, R. J., Mahowald, N., Winckler, G., Abe-Ouchi, A., O'ishi, R., Takemura, T., and Lee,
420 J. H.: The role of mineral-dust aerosols in polar temperature amplification, Nat. Clim. Change, 3, 487-491,
421 https://doi.org/10.1038/Nclimate1785, 2013.
422 Laskin, A., Cowin, J. P., and Iedema, M. J.: Analysis of Individual Environmental Particles using Modern Methods
423 of Electron Microscopy and X-ray Microanalysis, J. Electron. Spectrosc. Relat. Phenom., 150, 260-274,
424 https://doi.org/10.1016/j.elspec.2005.06.008, 2006.
425 Laskina, O., Morris, H. S., Grandquist, J. R., Qiu, Z., Stone, E. A., Tivanski, A. V., and Grassian, V. H.: Size Matters
426 in the Water Uptake and Hygroscopic Growth of Atmospherically Relevant Multicomponent Aerosol Particles,
427 J. Phys. Chem. A, 119, 4489-4497, https://doi.org/10.1021/jp510268p, 2015.
428 Li, W. J., Shao, L. Y., Zhang, D. Z., Ro, C. U., Hu, M., Bi, X. H., Geng, H., Matsuki, A., Niu, H. Y., and Chen, J.
429 M.: A review of single aerosol particle studies in the atmosphere of East Asia: morphology, mixing state,
430 source, and heterogeneous reactions, J. Cleaner Prod., 112, 1330-1349,
431 https://doi.org/10.1016/j.jclepro.2015.04.050, 2016.
432 Li, W. J., Teng, X. M., Chen, X. Y., Liu, L., Xu, L., Zhang, J., Wang, Y. Y., Zhang, Y., and Shi, Z. B.: Organic
433 Coating Reduces Hygroscopic Growth of Phase-Separated Aerosol Particles, Environ. Sci. Technol., 55,
434 16339-16346, https://doi.org/10.1021/acs.est.1c05901, 2021.
435 Ma, S. S., Pang, S. F., Li, J., and Zhang, Y. H.: A review of efflorescence kinetics studies on atmospherically relevant

436 particles, Chemosphere, 277, 130320, https://doi.org/10.1016/j.chemosphere.2021.130320, 2021.
437 Martin, S. T.: Phase Transitions of Aqueous Atmospheric Particles, Chem. Rev., 100, 3403-3453,
438 https://doi.org/10.1021/cr990034t, 2000.
439 Metzger, S., Dentener, F., Krol, M., Jeuken, A., and Lelieveld, J.: Gas/aerosol partitioning 2. Global modeling
440 results, Journal of Geophysical Research-Atmospheres, 107, ACH-17, https://doi.org/10.1029/2001jd001103,
441 2002a.
442 Metzger, S., Dentener, F., Pandis, S., and Lelieveld, J.: Gas/aerosol partitioning 1. A computationally efficient
443 model, Journal of Geophysical Research-Atmospheres, 107, D16, https://doi.org/10.1029/2001jd001102,
444 2002b.
445 Myhre, G., Bellouin, N., Berglen, T. F., Berntsen, T. K., Boucher, O., Grini, A., Isaksen, I. S. A., Johnsrud, M.,
446 Mishchenko, M. I., Stordal, F., and Tanre, D.: Comparison of the radiative properties and direct radiative effect
447 of aerosols from a global aerosol model and remote sensing data over ocean, Tellus B, 59, 115-129,
448 https://doi.org/10.1111/j.1600-0889.2006.00238.x, 2007.
449 Nandy, L., Yao, Y., Zheng, Z. H., and Riemer, N.: Water uptake and optical properties of mixed organic-inorganic
450 particles, Aerosol Sci. Technol., 55, 1398-1413, https://doi.org/10.1080/02786826.2021.1966378, 2021.
451 Nguyen, Q. T., Kjær, K. H., Kling, K. I., Boesen, T., and Bilde, M.: Impact of Fatty Acid Coating on the CCN
452 Activity of Sea Salt Particles, Tellus B: Chem. Phys. Meteorol., 69, 1304064,
453 https://doi.org/10.1080/16000889.2017.1304064, 2017.
454 Noziere, B.: Don't Forget the Surface, Science, 351, 1396-1397, https://doi.org/10.1126/science.aaf3253, 2016.
455 O'Brien, R. E., Wang, B. B., Kelly, S. T., Lundt, N., You, Y., Bertram, A. K., Leone, S. R., Laskin, A., and Gilles,
456 M. K.: Liquid-Liquid Phase Separation in Aerosol Particles: Imaging at the Nanometer Scale, Environ. Sci.
457 Technol., 49, 4995-5002, https://doi.org/10.1021/acs.est.5b00062, 2015.
458 Ohno, P. E., Qin, Y. M., Ye, J. H., Wang, J. F., Bertram, A. K., and Martin, S. T.: Fluorescence Aerosol Flow Tube
459 Spectroscopy to Detect Liquid-Liquid Phase Separation, ACS Earth Space Chem., 5, 1223-1232,
460 https://doi.org/10.1021/acsearthspacechem.1c00061, 2021.
461 Ohno, P. E., Brandao, L., Rainone, E. M., Aruffo, E., Wang, J. F., Qin, Y. M., and Martin, S. T.: Size Dependence
462 of Liquid-Liquid Phase Separation by in Situ Study of Flowing Submicron Aerosol Particles, J. Phys. Chem.
463 A, 127, 2967-2974, https://doi.org/10.1021/acs.jpca.2c08224, 2023.
464 Onasch, T. B., Siefert, R. L., Brooks, S. D., Prenni, A. J., Murray, B., Wilson, M. A., and Tolbert, M. A.: Infrared
465 Spectroscopic Study of The Deliquescence and Efflorescence of Ammonium Sulfate Aerosol as a Function of

Temperature, Journal of Geophysical Research-Atmospheres, 104, 21317-21326, https://doi.org/10.1029/1999jd900384, 1999.

Ott, E. J. E. and Freedman, M. A.: Influence of Ions on the Size Dependent Morphology of Aerosol Particles, ACS Earth Space Chem., 5, 2320-2328, https://doi.org/10.1021/acsearthspacechem.1c00210, 2021.

Ott, E. J. E., Kucinski, T. M., Dawson, J. N., and Freedman, M. A.: Use of Transmission Electron Microscopy for Analysis of Aerosol Particles and Strategies for Imaging Fragile Particles, Anal. Chem., 93, 11347-11356, https://doi.org/10.1021/acs.analchem.0c05225, 2021.

Peng, C., Chan, M. N., and Chan, C. K.: The Hygroscopic Properties of Dicarboxylic and Multifunctional Acids: Measurements and UNIFAC Predictions, Environ. Sci. Technol., 35, 4495-4501, https://doi.org/10.1021/es0107531, 2001.

Peng, C., Jing, B., Guo, Y. C., Zhang, Y. H., and Ge, M. F.: Hygroscopic Behavior of Multicomponent Aerosols Involving NaCl and Dicarboxylic Acids, J. Phys. Chem. A, 120, 1029-1038, https://doi.org/10.1021/acs.jpca.5b09373, 2016.

Peng, C., Chen, L., and Tang, M.: A Database for Deliquescence and Efflorescence Relative Humidities of Compounds with Atmospheric Relevance, Fundam. Res., 2, 578-587, https://doi.org/10.1016/j.fmre.2021.11.021, 2022.

Petters, M. D. and Kreidenweis, S. M.: A single parameter representation of hygroscopic growth and cloud condensation nucleus activity, Atmos. Chem. Phys., 7, 1961-1971, https://doi.org/10.5194/acp-7-1961-2007, 2007.

Pöhlker, C., Saturno, J., Krüger, M. L., Förster, J. D., Weigand, M., Wiedemann, K. T., Bechtel, M., Artaxo, P., and Andreae, M. O.: Efflorescence upon Humidification? X-ray Microspectroscopic in situ Observation of Changes in Aerosol Microstructure and Phase State upon Hydration, Geophys. Res. Lett., 41, 3681-3689, https://doi.org/10.1002/2014gl059409, 2014.

Pöschl, U.: Atmospheric Aerosols: Composition, Transformation, Climate and Health Effects, Angew. Chem. Int. Ed., 44, 7520-7540, https://doi.org/10.1002/anie.200501122, 2005.

Posfai, M., Axisa, D., Tompa, E., Freney, E., Bruintjes, R., and Buseck, P. R.: Interactions of Mineral Dust with Pollution and Clouds: An Individual-Particle TEM Study of Atmospheric Aerosol from Saudi Arabia, Atmos. Res., 122, 347-361, https://doi.org/10.1016/j.atmosres.2012.12.001, 2013.

Pye, H. O. T., Murphy, B. N., Xu, L., Ng, N. L., Carlton, A. G., Guo, H. Y., Weber, R., Vasilakos, P., Appel, K. W., Budisulistiorini, S. H., Surratt, J. D., Nenes, A., Hu, W. W., Jimenez, J. L., Isaacman-VanWertz, G., Misztal,

P. K., and Goldstein, A. H.: On the implications of aerosol liquid water and phase separation for organic aerosol mass, Atmos. Chem. Phys., 17, 343-369, https://doi.org/10.5194/acp-17-343-2017, 2017.

Reed, N. W., Wing, B. A., Tolbert, M. A., and Browne, E. C.: Trace H_2S Promotes Organic Aerosol Production and Organosulfur Compound Formation in Archean Analog Haze Photochemistry Experiments, Geophys. Res. Lett., 49, https://doi.org/10.1029/2021GL097032, 2022.

Riemer, N., Ault, A. P., West, M., Craig, R. L., and Curtis, J. H.: Aerosol Mixing State: Measurements, Modeling, and Impacts, Rev. Geophys., 57, 187-249, https://doi.org/10.1029/2018rg000615, 2019.

Römpp, A., Winterhalter, R., and Moortgat, G. K.: Oxodicarboxylic acids in atmospheric aerosol particles, Atmos. Environ., 40, 6846-6862, https://doi.org/10.1016/j.atmosenv.2006.05.053, 2006.

Roy, P., Mael, L. E., Makhnenko, I., Martz, R., Grassian, V. H., and Dutcher, C. S.: Temperature-Dependent Phase Transitions of Aqueous Aerosol Droplet Systems in Microfluidic Traps, ACS Earth Space Chem., 4, 1527-1539, https://doi.org/10.1021/acsearthspacechem.0c00114, 2020.

Ruehl, C. R. and Wilson, K. R.: Surface Organic Monolayers Control the Hygroscopic Growth of Submicrometer Particles at High Relative Humidity, J. Phys. Chem. A, 118, 3952-3966, https://doi.org/10.1021/jp502844g, 2014.

Ruehl, C. R., Davies, J. F., and Wilson, K. R.: An Interfacial Mechanism for Cloud Droplet Formation on Organic Aerosols, Science, 351, 1447-1450, https://doi.org/10.1126/science.aad4889, 2016.

Shiraiwa, M., Zuend, A., Bertram, A. K., and Seinfeld, J. H.: Gas-Particle Partitioning of Atmospheric Aerosols: Interplay of Physical State, Non-Ideal Mixing and Morphology, Physical Chemistry Chemical Physics, 15, 11441-11453, https://doi.org/10.1039/c3cp51595h, 2013.

Song, M., Marcolli, C., Krieger, U. K., Zuend, A., and Peter, T.: Liquid-Liquid Phase Separation and Morphology of Internally Mixed Dicarboxylic Acids/Ammonium Sulfate/Water Particles, Atmos. Chem. Phys., 12, 2691-2712, https://doi.org/10.5194/acp-12-2691-2012, 2012a.

Song, M., Marcolli, C., Krieger, U. K., Zuend, A., and Peter, T.: Liquid-Liquid Phase Separation in Aerosol Particles: Dependence on O:C, Organic Functionalities, and Compositional Complexity, Geophys. Res. Lett., 39, L19801, https://doi.org/10.1029/2012gl052807, 2012b.

Song, M., Maclean, A. M., Huang, Y. Z., Smith, N. R., Blair, S. L., Laskin, J., Laskin, A., DeRieux, W. S. W., Li, Y., Shiraiwa, M., Nizkorodov, S. A., and Bertram, A. K.: Liquid-Liquid Phase Separation and Viscosity within Secondary Organic Aerosol Generated from Diesel Fuel Vapors, Atmos. Chem. Phys., 19, 12515-12529, https://doi.org/10.5194/acp-19-12515-2019, 2019.

Song, M. J., Liu, P. F., Martin, S. T., and Bertram, A. K.: Liquid-Liquid Phase Separation in Particles Containing Secondary Organic Material Free of Inorganic Salts, Atmos. Chem. Phys., 17, 11261-11271, https://doi.org/10.5194/acp-17-11261-2017, 2017.

Stewart, D. J., Cai, C., Nayler, J., Preston, T. C., Reid, J. P., Krieger, U. K., Marcolli, C., and Zhang, Y. H.: Liquid-Liquid Phase Separation in Mixed Organic/Inorganic Single Aqueous Aerosol Droplets, J. Phys. Chem. A, 119, 4177-4190, https://doi.org/10.1021/acs.jpca.5b01658, 2015.

Takahama, S., Pathak, R. K., and Pandis, S. N.: Efflorescence Transitions of Ammonium Sulfate Particles Coated with Secondary Organic Aerosol, Environ. Sci. Technol., 41, 2289-2295, https://doi.org/10.1021/es0619915, 2007.

Ting, Y. C., Mitchell, E. J. S., Allan, J. D., Liu, D. T., Spracklen, D. V., Williams, A., Jones, J. M., Lea-Langton, A. R., McFiggans, G., and Coe, H.: Mixing State of Carbonaceous Aerosols of Primary Emissions from "Improved" African Cookstoves, Environ. Sci. Technol., 52, 10134-10143, https://doi.org/10.1021/acs.est.8b00456, 2018.

Tolocka, M. P. and Turpin, B.: Contribution of Organosulfur Compounds to Organic Aerosol Mass, Environ. Sci. Technol., 46, 7978-7983, https://doi.org/10.1021/es300651v, 2012.

Tong, Y. K., Meng, X. X. Y., Zhou, B., Sun, R., Wu, Z. J., Hu, M., and Ye, A. P.: Detecting the pH-dependent liquid-liquid phase separation of single levitated aerosol microdroplets via laser tweezers-Raman spectroscopy, Front. Phys., 10, https://doi.org/10.3389/fphy.2022.969921, 2022.

Unga, F., Choel, M., Derimian, Y., Deboudt, K., Dubovik, O., and Goloub, P.: Microscopic Observations of Core-Shell Particle Structure and Implications for Atmospheric Aerosol Remote Sensing, Journal of Geophysical Research-Atmospheres, 123, 13944-13962, https://doi.org/10.1029/2018jd028602, 2018.

Veghte, D. P., Bittner, D. R., and Freedman, M. A.: Cryo-Transmission Electron Microscopy Imaging of the Morphology of Submicrometer Aerosol Containing Organic Acids and Ammonium Sulfate, Anal. Chem., 86, 2436-2442, https://doi.org/10.1021/ac403279f, 2014.

Voorhees, P. W.: The Theory of Ostwald Ripening, J. Stat. Phys., 38, 231-252, https://doi.org/10.1007/Bf01017860, 1985.

Wang, N., Jing, B., Wang, P., Wang, Z., Li, J. R., Pang, S. F., Zhang, Y. H., and Ge, M. F.: Hygroscopicity and Compositional Evolution of Atmospheric Aerosols Containing Water-Soluble Carboxylic Acid Salts and Ammonium Sulfate: Influence of Ammonium Depletion, Environ. Sci. Technol., 53, 6225-6234, https://doi.org/10.1021/acs.est.8b07052, 2019.

Wang, W. H., Shao, L. Y., Mazzoleni, C., Li, Y. W., Kotthaus, S., Grimmond, S., Bhandari, J., Xing, J. P., Feng, X. L., Zhang, M. Y., and Shi, Z. B.: Measurement report: Comparison of wintertime individual particles at ground level and above the mixed layer in urban Beijing, Atmos. Chem. Phys., 21, 5301-5314, https://doi.org/10.5194/acp-21-5301-2021, 2021.

Wise, M. E., Martin, S. T., Russell, L. M., and Buseck, P. R.: Water Uptake by NaCl Particles Prior to Deliquescence and the Phase Rule, Aerosol Sci. Technol., 42, 281-294, https://doi.org/10.1080/02786820802047115, 2008.

Xiong, C., Chen, X. Y., Ding, X. L., Kuang, B. Y., Pei, X. Y., Xu, Z. N., Yang, S. K., Hu, H., and Wang, Z. B.: Reconsideration of Surface Tension and Phase State Effects on Cloud Condensation Nuclei Activity Based on the Atomic Force Microscopy Measurement, Atmos. Chem. Phys., 22, 16123-16135, https://doi.org/10.5194/acp-22-16123-2022, 2022.

Xu, L., Fukushima, S., Sobanska, S., Murata, K., Naganuma, A., Liu, L., Wang, Y. Y., Niu, H. Y., Shi, Z. B., Kojima, T., Zhang, D. Z., and Li, W. J.: Tracing the evolution of morphology and mixing state of soot particles along with the movement of an Asian dust storm, Atmos. Chem. Phys., 20, 14321-14332, https://doi.org/10.5194/acp-20-14321-2020, 2020.

Xu, W. Q., Chen, C., Qiu, Y. M., Li, Y., Zhang, Z. Q., Karnezi, E., Pandis, S. N., Xie, C. H., Li, Z. J., Sun, J. X., Ma, N., Xu, W. Y., Fu, P. Q., Wang, Z. F., Zhu, J., Worsnop, D. R., Ng, N. L., and Sun, Y. L.: Organic aerosol volatility and viscosity in the North China Plain: contrast between summer and winter, Atmos. Chem. Phys., 21, 5463-5476, https://doi.org/10.5194/acp-21-5463-2021, 2021.

Yang, H., Wang, N., Pang, S. F., Zheng, C. M., and Zhang, Y. H.: Chemical reaction between sodium pyruvate and ammonium sulfate in aerosol particles and resultant sodium sulfate efflorescence, Chemosphere, 215, 554-562, https://doi.org/10.1016/j.chemosphere.2018.10.062, 2019.

You, Y., Renbaum-Wolff, L., Carreras-Sospedra, M., Hanna, S. J., Hiranuma, N., Kamal, S., Smith, M. L., Zhang, X. L., Weber, R. J., Shilling, J. E., Dabdub, D., Martin, S. T., and Bertram, A. K.: Images Reveal that Atmospheric Particles can Undergo Liquid-Liquid Phase Separations, Proc. Natl. Acad. Sci. U.S.A., 109, 13188-13193, https://doi.org/10.1073/pnas.1206414109, 2012.

You, Y., Renbaum-Wolff, L., and Bertram, A. K.: Liquid–liquid phase separation in particles containing organics mixed with ammonium sulfate, ammonium bisulfate, ammonium nitrate or sodium chloride, Atmos. Chem. Phys., 13, 11723-11734, https://doi.org/10.5194/acp-13-11723-2013, 2013.

You, Y. and Bertram, A. K.: Effects of Molecular Weight and Temperature on Liquid-Liquid Phase Separation in Particles Containing Organic Species and Inorganic Salts, Atmos. Chem. Phys., 15, 1351-1365,

https://doi.org/10.5194/acp-15-1351-2015, 2015.

Zavacka, K., Nedela, V., Olbert, M., Tihlarikova, E., Vetrakova, L., Yang, X., and Heger, D.: Temperature and Concentration Affect Particle Size Upon Sublimation of Saline Ice: Implications for Sea Salt Aerosol Production in Polar Regions, Geophys. Res. Lett., 49, https://doi.org/10.1029/2021GL097098, 2022.

Zaveri, R. A., Easter, R. C., Fast, J. D., and Peters, L. K.: Model for Simulating Aerosol Interactions and Chemistry (MOSAIC), Journal of Geophysical Research-Atmospheres, 113, D13204, https://doi.org/10.1029/2007jd008782, 2008.

Zeng, G., Kelley, J., Kish, J. D., and Liu, Y.: Temperature-Dependent Deliquescent and Efflorescent Properties of Methanesulfonate Sodium Studied by ATR-FTIR Spectroscopy, J. Phys. Chem. A, 118, 583-591, https://doi.org/10.1021/jp405896y, 2014.

Zhang, J., Yuan, Q., Liu, L., Wang, Y. Y., Zhang, Y. X., Xu, L., Pang, Y., Zhu, Y. H., Niu, H. Y., Shao, L. Y., Yang, S. S., Liu, H., Pan, X. L., Shi, Z. B., Hu, M., Fu, P. Q., and Li, W. J.: Trans-Regional Transport of Haze Particles From the North China Plain to Yangtze River Delta During Winter, Journal of Geophysical Research-Atmospheres, 126, https://doi.org/10.1029/2020JD033778, 2021.

Zhang, J., Wang, Y. Y., Teng, X. M., Liu, L., Xu, Y. S., Ren, L. H., Shi, Z. B., Zhang, Y., Jiang, J. K., Liu, D. T., Hu, M., Shao, L. Y., Chen, J. M., Martin, S. T., Zhang, X. Y., and Li, W. J.: Liquid-Liquid Phase Separation Reduces Radiative Absorption by Aged Black Carbon Aerosols, Commun. Earth Environ., 3, 128, https://doi.org/10.1038/s43247-022-00462-1, 2022.

Zhang, Y., Chen, Y. Z., Lambe, A. T., Olson, N. E., Lei, Z. Y., Craig, R. L., Zhang, Z. F., Gold, A., Onasch, T. B., Jayne, J. T., Worsnop, D. R., Gaston, C. J., Thornton, J. A., Vizuete, W., Ault, A. P., and Surratt, J. D.: Effect of the Aerosol-Phase State on Secondary Organic Aerosol Formation from the Reactive Uptake of Isoprene-Derived Epoxydiols (IEPDX), Environ. Sci. Technol. Lett., 5, 167-174, https://doi.org/10.1021/acs.estlett.8b00044, 2018.

Zhang, Y. X., Zhang, Q., Yao, Z. L., and Li, H. Y.: Particle Size and Mixing State of Freshly Emitted Black Carbon from Different Combustion Sources in China, Environ. Sci. Technol., 54, 7766-7774, https://doi.org/10.1021/acs.est.9b07373, 2020.

Zhu, Y., Pang, S., and Zhang, Y.: Observations on the unique phase transitions of inorganics relevant due to gluconic acid in particles, Atmos. Environ., 288, 119313, https://doi.org/10.1016/j.atmosenv.2022.119313, 2022.